Drivers of cloud droplet number variability in the summertime Southeast United States

Aikaterini Bougiatioti[1,2], Athanasios Nenes[2,3,4], Jack J. Lin[2,a], Charles A. Brock[5], Joost A. de Gouw[5,6,b], Jin Liao[5,6,c,d], Ann M. Middlebrook[5], André Welti[5,6,e]

[1]Institute for Environmental Research & Sustainable Development, National Observatory of Athens, P. Penteli, GR-15236, Greece
[2]School of Earth & Atmospheric Sciences, Georgia Institute of Technology, Atlanta, GA 30332, USA
[3]Laboratory of Atmospheric Processes and their Impacts, School of Architecture, Civil & Environmental Engineering, École Polytechnique Fédérale de Lausanne, CH-1015, Lausanne, Switzerland
[4]Institute for Chemical Engineering Sciences, Foundation for Research and Technology Hellas, Patras, GR-26504, Greece
[5]Chemical Sciences Division, NOAA Earth System Research Laboratory, Boulder, CO, 80305, USA
[6]Cooperative Institute for Research in Environmental Sciences, Univ. of Colorado, Boulder, CO, 80309, USA
[a] now at: Nano and Molecular Systems Research Unit, Box 3000, FI-90014 University of Oulu, Oulu, Finland
[b] now at: Department of Chemistry and Biochemistry, University of Colorado Boulder, Boulder, CO, USA
[c] now at: Atmospheric Chemistry and Dynamic Laboratory, NASA Goddard Space Flight Center, Greenbelt, MD, USA
[d] now at: Universities Space Research Association, GESTAR, Columbia, MD, USA
[e] now at: Atmospheric Composition Research Unit, Finnish Meteorological Institute, Helsinki, Finland

Correspondence to: Aikaterini Bougiatioti (abougiat@noa.gr), Athanasios Nenes (athanasios.nenes@epfl.ch).

Abstract

Here we analyze regional scale data collected onboard the NOAA WP-3D aircraft during the 2013 Southeast Nexus (SENEX) campaign to study the aerosol-cloud droplet link and quantify the sensitivity of droplet number to aerosol number, chemical composition and vertical velocity. For this, the observed aerosol size distributions, chemical composition and vertical velocity distribution are introduced into a state-of-the-art cloud droplet parameterization to show that cloud maximum supersaturations in the region are low, ranging from 0.02 to 0.52% with an average of 0.14±0.05%. Based on these low values of supersaturation, the majority of activated droplets correspond to particles of dry diameter 90 nm and above. An important finding is that the standard deviation of the vertical velocity (σ_w) exhibits considerable diurnal variability (ranging from 0.16 m s^{-1} during nighttime to over 1.2 m s^{-1} during day) and it tends to covary with total aerosol number (N_a). This σ_w-N_a covariance amplifies the predicted response in cloud droplet number (N_d) to N_a increases by 3 to 5 times, compared to expectations based on N_a changes alone. This amplified response is important given that droplet formation is often velocity-limited, and therefore should normally be insensitive to aerosol changes. We also find that N_d cannot exceed a characteristic concentration that depends solely on σ_w. Correct consideration of σ_w and its covariance with time and N_a is important for fully understanding aerosol-cloud interactions and the magnitude of the aerosol indirect effect. Given that

40   model assessments of aerosol–cloud-climate interactions do not routinely evaluate for overall turbulence

41   or its covariance with other parameters, datasets and analyses such as the one presented here are of the

42   highest priority to address unresolved sources of hydrometeor variability, bias, and the response of droplet

43   number to aerosol perturbations.

1. Introduction

45   Atmospheric particles (aerosols) interact with incoming solar radiation and tend to cool the Earth, especially

46   over dark surfaces such as oceans and forests (Charlson et al., 1992). Aerosols also act as cloud

47   condensation nuclei (CCN), form droplets in clouds and indirectly affect climate by modulating

48   precipitation patterns and cloud radiative properties. Aerosol-cloud interactions constitute the most

49   uncertain aspects of anthropogenic climate change (Seinfeld et al., 2016). Studies often highlight the

50   importance of constraining the aerosol size distribution, particle composition and mixing state for predicting

51   CCN concentrations (Cubison et al., 2008; Quinn et al., 2008). Model assumptions often cannot consider

52   the full complexity required to comprehensively compute CCN – which together with other emissions and

53   process uncertainties lead to CCN prediction errors that can be significant (e.g., Fanourgakis et al., 2019).

54   Owing to the sublinear response of cloud droplet number concentration (N_d) to aerosol perturbations,

55   prediction errors in CCN generally result in errors in N_d which are less than those for CCN (Fanourgakis et

56   al., 2019). The sublinear response arises because elevated CCN concentration generally increases the

57   competition of the potential droplets for water vapor; this in turn depletes supersaturation and the N_d that

58   can eventually form (Reutter et al., 2009; Bougiatioti et al., 2016; Fanourgakis et al., 2019; Kalkavouras et

59   al., 2019). A critically important parameter is the vertical velocity, as it is responsible for generation of

60   supersaturation that drives droplet formation and growth. Droplet number variability may be driven

61   primarily by vertical velocity variations (Kacarab et al., 2020; Sullivan et al., 2019). Compared to aerosols,

62   vertical velocity is much less observed, constrained and evaluated in aerosol-cloud interaction studies,

63   hence may be a source of persistent biases in models (Sullivan et al., 2019).

64   The Southeast United States (SEUS) presents a particularly interesting location for studying regional

65   climate change, as it has not considerably warmed over the past 100 years – except during the last decade

66   (Carlton et al., 2018; Yu et al., 2014; Leibensperger et al., 2012a,b). These trends are in contrast with the

67   trends observed in most locations globally (IPCC 2013), and several hypotheses have been proposed to

68   explain this regional phenomenon, including the effect of involving short-lived climate forcers such as

69   secondary aerosols combined with the enhanced humidity in the region and their impact on clouds (Carlton

70   et al., 2018; Yu et al., 2014). Here, we analyze data collected during the Southeast Nexus of Air Quality

71   and Climate (SENEX) campaign in June-July 2013, which was the airborne component led by the National

72   Oceanic and Atmospheric Administration (NOAA), of a greater measurement campaign throughout the

73   SEUS, the Southeast Atmosphere Study (SAS; Carlton et al., 2018). Here we analyze data collected onboard

74   the NOAA WP-3D and apply a state-of-the-art droplet parameterization to determine the maximum

75   supersaturation and N_d achieved in cloudy updrafts, for all science flights with available number size

76   distribution and chemical composition data. We also determine the sensitivity of droplet formation to

77   vertical velocity and aerosol, with the purpose of understanding the drivers of droplet variability in the

78   boundary layer of the SEUS by obtaining regional-scale, representative values of the relationship between

79   the driving parameters and cloud droplet number.

80

81   **2. Methods**

82   *2.1 Aircraft instrumentation*

83   The analysis utilizes airborne, in situ data collected during the June-July 2013 SENEX mission, aboard the

84   National Oceanic and Atmospheric Administration (NOAA) WP-3D aircraft (typical airspeed ~100 m s^{-1})

85   based in Smyrna, Tennessee (36°00'32''N, 86°31'12''W). In total, twenty research flights were conducted.

86   Based on the availability of the relevant data described below, thirteen flights are analyzed in this work.

87   Table 1 provides a synopsis of the analyzed research flights where times are local (UTC-5). Detailed

88   information on the instrumentation and measurement strategy during the SENEX campaign is provided by

89   Warneke et al. (2016).

90   Dry particle number distributions from 4 - 7000 nm were measured using multiple condensation and optical

91   particle counters. 4-700 nm particles were measured by a nucleation mode aerosol size spectrometer

92   (NMASS; Warneke et al., 2016) and an ultra-high sensitivity aerosol spectrometer (UHSAS; Brock et al.,

93   2011), while for larger particles with dry diameters between 0.7 and 7.0 μm, a custom-built white-light

94   optical particle counter (WLOPC) was used (Brock et al., 2011).

95   Measurements of the composition of submicron (< 0.7 μm vacuum aerodynamic diameter) non-refractory

96   particles were made with a compact time-of-flight aerosol mass spectrometer (C-ToF-AMS; Aerodyne,

97   Billerica, Massachusetts, US) (Canagaratna et al., 2007; Kupc et al., 2018) customized for aircraft use, with

98   a 10 s time resolution (Warneke et al., 2016). Particles entering the instrument are focused and impacted

99   on a 600 °C inverted-cone vaporizer. The volatilized vapors are analyzed by electron ionization mass

100   spectrometry, providing mass loadings of sulfate, nitrate, organics, ammonium and chloride. For the C-

101   ToF-AMS, the transmission efficiency of particles between 100 and 700 nm is assumed to be 100% through

102   the specific aerodynamic focusing lens used while mass concentrations are calculated using a chemical

103   composition-dependent collection efficiency (Middlebrook et al., 2012; Wagner et al., 2015). The C-ToF-

104   AMS measures only non-refractory aerosol chemical composition, therefore this analysis provides mass

105   loadings of sulfate, nitrate, ammonium and organic constituents with a 10 s time resolution and neglects the
106   contribution of black carbon (BC). The calculation of the average volume fractions from the mass loading
107   follows that of Moore et al. (2012). An average organic density of 1.4 g cm^{-3} is used, characteristic of aged
108   aerosol (Moore et al., 2011; Lathem et al., 2013) while for the inorganic species the respective densities are
109   used, assuming the aerosol to be internally mixed (Lance et al., 2009; Bougiatioti et al., 2009; Wang et al.,
110   2010)

111   The aircraft was equipped by the NOAA Aircraft Operations Center (AOC) flight facility with a suite of
112   instruments to provide information on exact aircraft position as well as numerous meteorological
113   parameters (Warneke et al., 2016). The analysis in this work makes use of vertical wind velocity, aircraft
114   pressure altitude, and ambient temperature, pressure and relative humidity (RH) provided by NOAA AOC.
115   The location of the instrumentation on the aircraft is described elsewhere (Warneke et al., 2016). For
116   measurements inside the fuselage, a low turbulence inlet (Wilson et al., 2004) and sampling system (Brock
117   et al., 2011; 2016a) was used to decelerate the sample flow to the instruments. The C-ToF-AMS was
118   connected downstream of an impactor with 50% efficiency at a 1.0 μm aerodynamic diameter (PM1) cut-
119   point (Warneke et al., 2016).

120   *2.2 Aerosol hygroscopicity parameter*

121   The aerosol hygroscopicity parameter (Petters and Kreidenweis, 2007), κ, is calculated assuming a mixture
122   of an organic and inorganic component with volume fractions ε_{org}, ε_{inorg} and characteristic hygroscopicities
123   κ_{org}, κ_{inorg}, respectively ($\kappa=\varepsilon_{inorg}\kappa_{inorg}+\varepsilon_{org}\kappa_{org}$). The organic and inorganic volume fraction are derived from
124   the C-ToF-AMS data. Since throughout the summertime SEUS, aerosol inorganic nitrate mass and volume
125   fraction are very low (Weber et al., 2016; Fry et al., 2018), κ_{inorg} =0.6, representative for ammonium sulfate,
126   is used. For the organic fraction, a hygroscopicity value of κ_{org}=0.14 is used, based on concurrent
127   measurements conducted at the ground site of the SAS at the rural site of Centreville, Alabama (Cerully et
128   al., 2015). This value is also in accordance with the cumulative result of studies conducted in the Southeast
129   US using measurements of droplet activation diameters in subsaturated regimes, providing κ_{org} of > 0.1
130   (Brock et al., 2016a).

131   *2.3 Cloud droplet number and maximum supersaturation*

132   Using the observed aerosol number size distribution (1 s time resolution) and the hygroscopicity derived
133   from the chemical composition measurements (10 s time resolution) and vertical velocity, we calculate the
134   (potential) cloud droplet number (N_d) and maximum supersaturation (S_{max}) that would form in clouds in the
135   airmasses sampled. Droplet number and maximum supersaturation calculations are carried out using an

136 approach similar to that of Bougiatioti et al. (2017) and Kalkavouras et al. (2019) with the sectional
137 parameterization of Nenes and Seinfeld (2003), later improved by Barahona et al. (2010) and Morales
138 Betancourt and Nenes (2014a). A sectional representation of the size distribution is used for each 1-s data
139 point (e.g. for Flight 5, n=23213 data points). Given that chemical composition is provided with a 10 s time
140 resolution, the same hygroscopicity values are used for 10 successive size distributions throughout the
141 flight. Temperature and pressure required for droplet number calculations are obtained from the NOAA
142 AOC flight facility dataset.

143 Given that vertical velocity varies considerably inside the boundary layer, we obtain a droplet number that
144 is representative of the vertical velocity distribution – the average concentration that results from integrating
145 over the distribution (probability density function, PDF) of observed updraft velocities. To accomplish this,
146 each flight is divided into segments where the aircraft flew at a constant height. For each segment, only the
147 non-negative vertical velocities are fit to the positive half of a Gaussian distribution around a mean of zero
148 and standard deviation σ_w. Only positive vertical velocities ("updrafts") were used in this fit, as they are the
149 part of the vertical velocity spectrum that is responsible for cloud droplet formation. The σ_w values derived
150 from the level leg segments are then averaged into one single σ_w value to represent each flight. The PDF-
151 averaged droplet number concentration is then obtained using the "characteristic velocity" approach of
152 Morales and Nenes (2010), where applying the droplet parameterization at a single "characteristic" velocity,
153 $w^*=0.79\sigma_w$ (Morales and Nenes, 2010) gives directly the PDF-averaged value. The flight-averaged σ_w and
154 subsequently the respective w^* is applied to each size distribution measured. Apart from its theoretical basis,
155 this methodology has shown to provide good closure with observed droplet numbers in ambient clouds (e.g.
156 Kacarab et al., 2020).

157 In determining σ_w, we consider horizontal segments most likely to be in the boundary layer. 91% of the
158 segments are below 1000 m above sea level (mean altitude ~700 m; Table 2 and SP3 for all flights), within
159 the boundary layer in the summertime US (Seidel et al., 2012). Also according to Wagner et al. (2015) the
160 mixed layer height in the area during the measurements had a median of 1.2 km while during nighttime
161 values are <0.5 km (Seidel et al., 2012). The vertical velocity distributions observed gave σ_w =0.97±0.21 m
162 s^{-1} for daytime flights, and σ_w =0.23±0.04 m s^{-1} for nighttime flights (Table 2 and SP3).
163 Potential droplet formation is evaluated at four characteristic velocities w^* that cover the observed range in
164 σ_w, namely 0.1, 0.3, 0.6, and 1 m s^{-1}. The σ_w = 0.3 m s^{-1} case is most representative of nighttime conditions,
165 while σ_w = 1 m s^{-1} should is most representative of the daytime boundary layer (Table 3).
166 We also compute the variance of the derived N_d, estimated from the sensitivity to changes in aerosol number
167 concentration N_a, κ and σ_w, expressed by the partial derivatives $\partial N_d/\partial N_a$, $\partial N_d/\partial \kappa$ and $\partial N_d/\partial \sigma_w$ computed

168 from the parameterization using a finite difference approximation (Bougiatioti et al., 2017; Kalkavouras et
169 al., 2019) using:

$$\sigma^2 N_d = \left(\frac{\overline{\partial N_d}}{\partial N_a}\ \sigma N_a\right)^2 + \left(\frac{\overline{\partial N_d}}{\partial \kappa}\ \sigma \kappa\right)^2 + \left(\frac{\overline{\partial N_d}}{\partial \sigma_w}\ \sigma w\right)^2 \qquad (1)$$

172 These sensitivities, together with the observed variance in N_a, κ, and σ_w are also used to attribute droplet
173 number variability to variations in the respective aerosol and vertical velocity parameters following the
174 approach of Bougiatioti et al. (2017) and Kalkavouras et al. (2019):

$$\varepsilon_{N\alpha} = \frac{\left(\frac{\overline{\partial N_d}}{\partial N_a}\sigma N_a\right)^2}{\sigma^2 N_d}, \varepsilon_\kappa = \frac{\left(\frac{\overline{\partial N_d}}{\partial \kappa}\sigma \kappa\right)^2}{\sigma^2 N_d}, \varepsilon_{\sigma w} = \frac{\left(\frac{\overline{\partial N_d}}{\partial \sigma_w}\sigma w\right)^2}{\sigma^2 N_d} \qquad (2)$$

3. Results and Discussion

3.1. Particle composition and size distribution

180 For the determination of the different aerosol species present, neutral and acidic sulfate salts are
181 distinguished by the molar ratio of ammonium to sulfate ions in the aerosol. A molar ratio higher than 2
182 indicates the presence of only ammonium sulfate, while values between 1 and 2 indicate a mixture of
183 ammonium sulfate and bisulfate (Seinfeld and Pandis, 1998). For most flights, the molar ratio of ammonium
184 versus sulfate was above 2 (mean value 2.41±0.72 and median of 2.06). For the nighttime flights, the values
185 were somewhat lower (mean value 1.91±0.42 and median of 1.85). Nevertheless, ammonium sulfate is
186 always the predominant sulfate salt. Organic mass fractions for the SENEX research flights are provided in
187 Table 1. Overall, organic aerosol dominated the composition during all flights, contributing 66%-75% of
188 the total aerosol volume. Most of the remaining aerosol volume consisted of ammonium sulfate, ranging
189 from 12%-39% (with a mean of 23%±6%). The organic mass fraction during the flights varied with height
190 (see Figure 1). This vertical variability of the chemical composition can have a strong impact on droplet
191 number within the boundary layer, as air masses from aloft may descend and interact with that underneath.
192 Figure 1 represents the organic mass fractions during Flights 6, 12 and 16, with all flights provided in the
193 supplementary material (Figure S1). The dashed line represents the boundary layer for daytime (1200 m;
194 Wagner et al., 2015) and for nighttime (500 m; Seidel et al., 2012). The lowest organic mass fractions were
195 observed during Flight 12 (36%±10% with values almost two-fold higher for altitudes >3000 m, Figure 1b)
196 while the highest organic mass fractions were observed during flights over predominantly rural areas
197 (Flights 5, 10, and 16 (Figure 1c)). During Flight 5 the organic mass fraction was high (68%±5%), with the
198 highest values found in the free troposphere at altitudes >3000 m, as was the case for 4 other flights (5/3 in
199 total, Fig. S1). High organic mass fractions were also found during nighttime Flight 9 that included portions

200   of the Atlanta metropolitan area, with values up to 78%. The impact of the aerosol composition variability

201   on droplet number is discussed in section 3.2.

202   The predominance of the organic fraction is also reflected in the hygroscopicity parameter values, with an

203   overall $\kappa = 0.25 \pm 0.05$, close to the proposed global average of 0.3 (Pringle et al., 2010). The highest values

204   of κ, as expected are observed during flights exhibiting the lowest organic mass fraction, namely Flight 12

205   with a $\kappa = 0.39$ (Table 1). The rest of the κ-values are close to the overall value of 0.25, corresponding to

206   an organic mass fraction of around 0.60.

207   Median aerosol size distributions and the respective total aerosol number are obtained from the median and

208   interquartile range in each size bin from the aerosol size distribution measurements during segments where

209   the aircraft flew at a constant height. Aerosol size distributions and changes in them during each flight are

210   crucial as they are used as input for the droplet number parameterization. Overall, N_a ranged from around

211   500 to over 100000 cm^{-3} with number size distributions varying markedly over the course of a flight (Figure

212   2). Free tropospheric distributions exhibited characteristics of a bimodal distribution with a prominent broad

213   accumulation mode peak (80-200 nm) and an Aitken mode peak (30-60 nm) (Fig. 2a) while boundary layer

214   size distributions exhibited a more prominent accumulation mode (Fig. 2b). There was considerable

215   variability in the contributions of the nucleation, Aitken, and accumulation modes to total N_a, depending on

216   altitude and proximity to aerosol sources (Fig. 2c). Nevertheless, the modal diameters did not vary

217   considerably, dictating that mostly particles in the same mode will activate, depending on the developed

218   supersaturation. Distributions during nighttime flights exhibited similar total N_a and variability between

219   them; nevertheless, size distributions were more complex - exhibiting up to three distinct modes (20-40,

220   70-100 and 130-200 nm; Fig. 2d).

221   *3.2 Potential cloud droplet number and maximum supersaturation*

222   We first focus on calculation of the potential N_d and S_{max} for data from all thirteen research flights and for

223   the four prescribed values σ_w that represent the observed range. These calculations are helpful in

224   understanding the sensitivity of droplet formation to N_a and κ for all the airmasses sampled – without

225   considering the added variability induced by changes in turbulence expressed by σ_w (considered later).

226   Results from this analysis are provided in Table 3. The highest N_d were found for Flights 6 and 10, which

227   correspond to ambient conditions with the highest N_a, consistent with the sampling of the Atlanta urban

228   environment. For a given σ_w, the variance of N_d is predominantly caused by changes in N_a rather than

229   changes in hygroscopicity (i.e., chemical composition). The highest influence of κ to N_d variability is found

230   for Flight 18 (12% and 35% for 0.1 and 0.3 m s^{-1}, respectively), during which N_a was the lowest, and the

231   organic mass fraction was ~50%. The contribution of κ to the N_d variability is as high as 37% (for 0.6 m s^{-1}

232   ^{1}); despite this large contribution, droplet formation is usually considerably more sensitive to changes in

7

aerosol concentration than to variations in composition. Overall, the relative contribution of the hygroscopicity to the variation of N_d increases from 5±3% for σ_w =0.1 m s^{-1}, to 12.3±8% for σ_w =0.3 m s^{-1}, to 14.5±10% for σ_w =0.3 m s^{-1} and 16.5±9% for σ_w =1 m s^{-1}. As σ_w increases, so does supersaturation and consequently N_d . On average, N_d increases by 62% as σ_w increased from 0.1 to 0.3 m s^{-1}, 70% as σ_w increased from 0.3 to 0.6 m s^{-1} and another 39% as σ_w increased from 0.6 to 1 m s^{-1}. Tripling σ_w from 0.1 to 0.3 m s^{-1} results in 31% increase in S_{max}, while doubling σ_w from 0.3 to 0.6 m s^{-1} results in 26.2% increase in S_{max} and a further σ_w increase to 1 m s^{-1} leads to an additional 20.7% increase in S_{max}.

Considering the changes in vertical velocity between flights (Table 4), we observe that average σ_w during daytime varied little between flights and was large, ranging between 0.85 and 1.2 m s^{-1} with a mean of 0.97±0.21 m s^{-1}. Under such conditions, water availability during droplet formation is aerosol-limited, so that N_d is sensitive to N_a. The degree of water availability is expressed by the S_{max}, which for all the evaluated SENEX data, is 0.14±0.05%. This level of maximum supersaturation activates particles of roughly >90 nm diameter (e.g., accumulation mode particles) into cloud droplets. The highest S_{max} ranged from 0.2 to 0.3% and was found during flights which exhibited large and highly variable σ_w (Flights 4, 5, 12 and 19) while the lowest S_{max} was below 0.10% and was found during nighttime flights (Flights 9, 15 and 16). Contrasts in droplet formation between day and nighttime conditions may be driven primarily by the total aerosol number in the accumulation mode, and not be affected by ultrafine particles.

The large diurnal variability in σ_w (from 0.3 m s^{-1} at night to 1.0 m s^{-1} at day) contributes considerably to the diurnal variability in N_d. To understand the relative importance of all parameters affecting droplet formation (σ_w, N_a, κ) we estimate their contribution to the total variability in N_d based on the variances of κ, N_a and σ_w and the sensitivity of droplet formation to those parameters. The results of the analysis are summarized in Table 4. The σ_w variation during nighttime, although small (always less than 10%), consistently remains an important contributor to N_d variability, because droplet formation tends to be in the updraft velocity-limited regime. At higher values of σ_w (Table 4), the contribution of N_a variability becomes a relatively dominant contributor to N_d variability.

Another way to express the importance of vertical velocity and aerosol number for the levels of droplet number is to compare flights where aerosol number or σ_w vary in a similar way. For this, we focus on two day/night flight pairs (Flights 5 and 15, and Flights 6 and 9), shown in Fig. 3. The first pair of flights were conducted over a rural area under moderate aerosol number conditions, while the second pair exhibited somewhat higher aerosol numbers owing to its proximity to the Atlanta metropolitan area. The size of the markers in Fig.3 represents the potential number of droplets in clouds forming in each airmass sampled, while their color reflects the respective total aerosol number. In both pairs of flights, σ_w varies about the same between night and day (Table 4). For the Flights 5, 15 pair, the difference in N_d between day and night

266   (which is 69% higher during daytime) is driven primarily by aerosol concentrations with κ having limited

267   influence (69% by N_a and 7% from κ) and only 24% by σ_w. For nighttime (Flight 15), the majority of

268   variability in N_d is driven again by aerosol concentrations and to a limited extent by κ (51% by N_a and 7%

269   from κ) and 42% by σ_w. For the second pair of night/day flights (Flights 6, 9), N_a is on average similar, σ_w

270   varies by a factor of 4.0 between day and night and κ varies by 13%.

271   The difference in N_d between day and night (where daytime values are 72.1% higher than nighttime) is

272   almost equally driven by N_a and σ_w changes during the day (54% and 43% respectively), while

273   predominantly driven by N_a during the night (76%; Table 4). Overall, in the proximity of an urban

274   environment with higher aerosol concentrations, 57% of the N_d variability is driven by aerosol (N_a and κ)

275   during the day and 83% during the night.

276   Figure 4 shows N_d relative to N_a for flights conducted in the two aforementioned areas, during day (Flights

277   5 and 15) and night (Flights 6 and 9). For high enough N_a, N_d becomes insensitive to additional amounts of

278   aerosol and reaches a "limiting" N_d, which Kacarab et al. (2020) denotes as N_d^{lim}. This limit in N_d is reached

279   when the competition for water vapor to form droplets is high enough to inhibit the formation of droplets

280   with further increase in N_a. The intense competition for water vapor is reflected in the low value of S_{max},

281   which drops below 0.1% when N_d is in the vicinity of N_d^{lim} (Figure 4). The availability of water vapor during

282   droplet formation is driven by σ_w, hence droplet formation is limited by σ_w and thus by velocity, when N_d

283   approaches N_d^{lim}. Figure 5 illustrates these effects, by presenting the relationship between N_a and N_d for

284   "low" w^* (<0.25 ms^{-1}; upper panel), "medium" w^* (0.5-0.7 ms^{-1}; middle panel), and "high" w^* (0.75-1 ms^{-}

285   ^{1}; lower panel) for all flights. Under low $w*$ conditions, changes in N_a do not result in an large change in

286   N_d, so its value corresponds to N_{lim}. When w^* increases to "medium" values (Figure 5b), then N_d becomes

287   sensitive to N_a, which is further amplified at "high" values of w^* (Figure 5c). The covariance of aerosol

288   number and vertical velocity (Figure S3) means that the latter significantly enhances the inherent response

289   of N_d to N_a, which points to the importance of constraining vertical velocity and its variance to correctly

290   capture the aerosol-cloud droplet relationship in any model. The covariance, also observed in other

291   environments (e.g., Kacarab et al., 2020) may be a result of more effective convective transfer of aerosol-

292   rich air to cloud forming regions, but requires further investigation.

293   Analysis of Figure 4 also shows that N_d^{lim} varies between 1200 cm^{-3} during day and around 350 cm^{-3} during

294   night, which points to its strong dependence on σ_w. Indeed, when the N_d^{lim} for all flights (except Flights 4,

295   12, for which insufficient aerosol is present to reach N_d^{lim}) is expressed as a function of σ_w, a remarkable

296   correlation emerges between the two parameters (Figure 6). Even more interesting is that this relationship

297   is quantitiatively similar to the corresponding N_d^{lim} - σ_w relationship Kacarab et al. (2020) found for biomass

298   burning - influenced boundary layer clouds in the Southeast Atlantic. The implication of the N_d^{lim} - σ_w

299 relationship, and its potential universality, is that when N_d approaches N_d^{lim}, its variability is a reflection of

300 vertical velocity variability alone, not variability in N_a. This opens up the possibility to infer the vertical

301 velocity distribution from the droplet number concentration in regions where considerable amounts of

302 aerosol are present.

303

304 **4. Summary and Conclusions**

305 Measurements of vertical wind velocity, ambient temperature, humidity, aerosol number size distribution

306 and composition in the SEUS obtained during the SENEX 2013 project are used to analyze the drivers of

307 droplet formation. Overall, 13 research flights are studied, covering environments over sectors with

308 different aerosol sources, aerosol number, size distribution, chemical composition and updraft velocity.

309 Aerosol volume is largely dominated by an organic fraction resulting in an estimated hygroscopicity of

310 0.25±0.05.

311 Based on the calculation of cloud droplet number concentration (N_d) and maximum supersaturation (S_{max}),

312 we find that at the regional scale, N_d variability is largely driven by fluctuations in N_a (Table 4), in

313 accordance with other recent studies (e.g., Fanourgakis et al., 2019; Kalkavouras et al., 2019; Kacarab et

314 al., 2020). Nonetheless, N_d levels are also sensitive to vertical velocity variations, σ_w; a factor of 4.0 change

315 in σ_w on its own may lead to an almost proportional change in N_d (factor of 3.6). These responses however

316 occur over the diurnal timescale, during which N_a also changes; the covariance between σ_w with N_a enhances

317 the apparent response of N_d to changes in N_a levels by a factor of 5 (Figure 4). In "cleaner" environments

318 where total aerosol number is not impacted by local sources, the relative response of N_d to σ_w is almost

319 twice as great at night than during the day (24% for daytime Flight 5 vs. 42% for nighttime Flight 15). On

320 the other hand, the relative response of N_d to N_a is slightly lower during the night than during the day (51%

321 at night vs. 69% during the day). In environments with elevated concentrations of accumulation-mode

322 particles, the majority of N_d variations can be attributed to changes in N_a and to a lesser extent to changes

323 in σ_w . Variations in chemical composition (expressed by κ) do not contribute substantially to droplet

324 number variability in most cases. As expected, S_{max} partially mitigates the response of N_d to N_a. Overall,

325 maximum supersaturation levels remain quite low (0.14±0.05%) with the lowest levels (0.05±0.1%)

326 estimated closest to surface. As a result, particles with diameters >90 nm were the most substantial

327 contributors to CCN.

328 Our analysis also reveals the importance of the variance in vertical velocity as a key driver of cloud droplet

329 formation and its variability in the region. When the boundary layer turbulence is low (e.g. during

330 nighttime) and water vapor supersaturations are low, σ_w and as a consequence vertical velocity variability,

331 can be as important of a contributor to N_d as is N_a. Even for situations with both high σ_w and N_a, the large

332 σ_w enables enough water vapor availability to activate significant numbers of particles to cloud droplets.

333 On average, the two variables (N_a and σ_w) contribute almost equally to the variability in N_d and together

334 account for more than 90% of variability. This finding is consistent with recent modeling studies noting the

335 importance of vertical velocity variability as a driver of the temporal variability of global hydrometeor

336 concentration (Morales Betancourt and Nenes, 2014b; Sullivan et al., 2016). Furthermore, the N_d response

337 from changes in N_a is magnified up to 5 times by correlated changes in σ_w. A similar situation was seen in

338 marine boundary layers influenced by biomass burning in the Southeast Atlantic (Kacarab et al., 2020).

339 Finally, we identify an upper limit to the number of droplets that can form in clouds which depends only

340 on σ_w. This upper limit value tends to be achieved near the surface, where N_a tends to be higher. Whenever

341 N_d approach this upper limit, observed droplet variability is driven by σ_w and as a consequence by vertical

342 velocity changes only.

343 Many aspects of warm cloud physics and especially droplet formation have known for decades. Ensuring

344 that global models simulate N_d for the "right reasons" (i.e., aerosol variability and/or vertical velocity

345 variability) is critical for constraining aerosol-cloud-climate interactions. Our study provides important

346 constraints on the relationships between σ_w, N_a, potential N_d, and S_{max}, and shows the importance of

347 covariance between σ_w and N_a in controlling the maximum N_d that can result from a given value of σ_w.

348 Given that global model assessments of aerosol–cloud-climate interactions do not evaluate for vertical

349 velocity or its covariance with other parameters, our work shows that this omission can lead to an

350 underappreciated source of hydrometeor variability and bias, and to a biased response of droplet number to

351 aerosol perturbations.

352

353 **Data Availability:** The data used in this study can be downloaded from the NOAA public data repository

354 at https://www.esrl.noaa.gov/csd/projects/senex/. The Gaussian fits used for determining σ_w and the droplet

355 parameterization used for the calculations in the study are available from athanasios.nenes@epfl.ch upon

356 request.

357

358 **Author Contributions:** AB and AN designed and initiated the study. Analysis methodology and software

359 were provided by AN. The analysis was carried out by AB and AN, with comments from JJL, CB, AMM.

360 Data curation was provided by AB, JJL, CB, JAG, JL, AMM, AW. The manuscript was written by AB and

361 AN with additional comments provided by JJL, CB, AW, AMM. All authors reviewed the manuscript.

362

372

373 **References**

374 Barahona, D., West, R.E.L., Stier, P., Romakkaniemi, S., Kokkola, H., and Nenes, A.: Comprehensively

375 accounting for the effect of giant CCN in cloud activation parameterizations, Atmos. Chem. Phys., 10,

376 2467–2473, https://doi.org/10.5194/acp-10-2467-2010, 2010.

377 Bougiatioti, A., Fountoukis, C., Kalivitis, N., Pandis, S. N., Nenes,A., and Mihalopoulos, N.: Cloud

378 condensation nuclei measure-ments in the marine boundary layer of the eastern Mediterranean:CCN

379 closure and droplet growth kinetics, Atmos. Chem. Phys.,9, 7053–7066,doi:10.5194/acp-9-7053-

380 2009, 2009.

381 Bougiatioti, A., Bezantakos, S., Stavroulas, I., Kalivitis, N., Kokkalis, P., Biskos, G., Mihalopoulos, N.,

382 Papayannis, A., and Nenes, A.: Biomass-burning impact on CCN number, hygroscopicity and cloud

383 formation during summertime in the eastern Mediterranean, Atmos. Chem. Phys., 16, 7389–7409,

384 https://doi.org/10.5194/acp-16-7389-2016, 2016.

385 Bougiatioti, A., Argyrouli, A., Solomos, S., Vratolis, S., Eleftheriadis, K., Papayannis, A., and Nenes, A.:

386 CCN activity, variability and influence on droplet formation during the HygrA-Cd campaign in

387 Athens, Atmosphere, 8, 108, https://doi.org/10.3390/atmos8060108, 2017.

388 Brock, C. A., Cozic, J., Bahreini, R., Froyd, K. D., Middlebrook, A. M., McComiskey, A., Brioude, J.,

389 Cooper, O. R., Stohl, A., Aikin, K. C., de Gouw, J. A., Fahey, D. W., Ferrare, R. A., Gao, R. S., Gore,

390 W., Holloway, J. S., Hübler, G., Jefferson, A., Lack, D. A., Lance, S., Moore, R. H., Murphy, D. M.,

391 Nenes, A., Novelli, P. C., Nowak, J. B., Ogren, J. A., Peischl, J., Pierce, R. B., Pilewskie, P., Quinn,

392 P. K., Ryerson, T. B., Schmidt, K. S., Schwarz, J. P., Sodemann, H., Spackman, J. R., Stark, H.,

393 Thomson, D. S., Thornberry, T., Veres, P., Watts, L. A., Warneke, C., and Wollny, A. G.:

394 Characteristics, sources, and transport of aerosols measured in spring 2008 during the aerosol,

395   radiation, and cloud processes affecting Arctic Climate (ARCPAC) Project, Atmos. Chem. Phys., 11,

396   2423–2453, 2011.

397 Brock, C. A., Wagner, N. L., Anderson, B. E., Attwood, A. R., Beyersdorf, A., Campuzano-Jost, P.,

398   Carlton, A. G., Day, D. A., Diskin, G. S., Gordon, T. D., Jimenez, J. L., Lack, D. A., Liao, J., Markovic,

399   M. Z., Middlebrook, A. M., Ng, N. L., Perring, A. E., Richardson, M. S., Schwarz, J. P., Washenfelder,

400   R. A., Welti, A., Xu, L., Ziemba, L. D., and Murphy, D. M.: Aerosol optical properties in the

401   southeastern United States in summer – Part 1: Hygroscopic growth, Atmos. Chem. Phys., 16, 4987-

402   5007, https://doi.org/10.5194/acp-16-4987-2016, 2016.

403 Canagaratna, M. R., Jayne, J. T., Jimenez, J. L., Allan, J. D., Alfarra,M. R., Zhang, Q., Onasch, T. B.,

404   Drewnick, F., Coe, H., Middlebrook, A., Delia, A., Williams, L. R., Trimborn, A. M., Northway, M.

405   J., DeCarlo, P. F., Kolb, C. E., Davidovits, P., and Worsnop, D. R.: Chemical and microphysical

406   characterization of ambient aerosols with the aerodyne aerosol mass spectrometer, Mass Spectrom.

407   Rev., 26, 185–222, 2007.

408 Carlton, A.G., J.A. de Gouw, J.L. Jimenez, J.L. Ambrose, A.R. Attwood, S. Brown, K.R. Baker, C. Brock,

409   R.C. Cohen, S. Edgerton, C. Farkas, D. Farmer, A.H. Goldstein, L. Gratz, A. Guenther, S. Hunt, L.

410   Jaeglé, D.A. Jaffe, J. Mak, C. McClure, A. Nenes, T.K.V. Nguyen, J.R. Pierce, S. de Sa, N.E. Selin,

411   V. Shah, S. Shaw, P.B. Shepson, S. Song, J. Stutz, J. Surratt, B.J. Turpin, C. Warneke, R.A.

412   Washenfelder, P.O. Wennberg, and Xianling Zhou: A synthesis of the southeast atmosphere studies:

413   coordinated investigation of fundamental atmospheric chemistry questions, Bull. Am. Meteor. Soc.,

414   https://doi.org/10.1175-BAMS-D-16-0048.1, 2018.

415 Charlson, R.J., Schwartz, S.E., Hales, J.M., Cess, J.M., Coakley Jr., J.A., Hansen, J.E., and Hofmann, D.J.:

416   Climate forcing by anthropogenic aerosol, Science, 225, 5043, 423-430, doi:

417   10.1126/science.255.5043.423, 1992.

418 Cubison, M. J., Ervens, B., Feingold, G., Docherty, K. S., Ulbrich, I. M., Shields, L., Prather, K., Hering,

419   S., and Jimenez, J. L.: The influence of chemical composition and mixing state of Los Angeles urban

420   aerosol on CCN number and cloud properties, Atmos. Chem. Phys., 8, 5649-5667,

421   https://doi.org/10.5194/acp-8-5649-2008, 2008.

422 DeCarlo, P. F., Kimmel, J. R., Trimborn, A., Northway, M. J., Jayne, J. T., Aiken, A. C., Gonin, M., Fuhrer,

423   K., Horvath, T., Docherty, K. S., Bates, D. R., and Jimenez, J. L.: Field-deployable, high-resolution,

424   time-of-flight aerosol mass spectrometer, Anal. Chem., 78, 8281–8289,

425   https://doi.org/doi:8210.1021/ac061249n, 2006.

426 Fanourgakis, G. S., Kanakidou, M., Nenes, A., Bauer, S. E., Bergman, T., Carslaw, K. S., Grini, A.,

427   Hamilton, D. S., Johnson, J. S., Karydis, V. A., Kirkevåg, A., Kodros, J. K., Lohmann, U., Luo, G.,

428   Makkonen, R., Matsui, H., Neubauer, D., Pierce, J. R., Schmale, J., Stier, P., Tsigaridis, K., van Noije,

429   T., Wang, H., Watson-Parris, D., Westervelt, D. M., Yang, Y., Yoshioka, M., Daskalakis, N., Decesari,

430   S., Gysel-Beer, M., Kalivitis, N., Liu, X., Mahowald, N. M., Myriokefalitakis, S., Schrödner, R.,

431   Sfakianaki, M., Tsimpidi, A. P., Wu, M., and Yu, F.: Evaluation of global simulations of aerosol

432   particle and cloud condensation nuclei number, with implications for cloud droplet formation, Atmos.

433   Chem. Phys., 19, 8591–8617, https://doi.org/10.5194/acp-19-8591-2019, 2019.

434 Fry, J. L., Brown, S. S., Middlebrook, A. M., Edwards, P. M., Campuzano-Jost, P., Day, D. A., Jimenez,

435   J. L., Allen, H. M., Ryerson, T. B., Pollack, I., Graus, M., Warneke, C., de Gouw, J. A., Brock, C. A.,

436   Gilman, J., Lerner, B. M., Dubé, W. P., Liao, J., and Welti, A.: Secondary organic aerosol (SOA)

437   yields from NO3 radical + isoprene based on nighttime aircraft power plant plume transects, Atmos.

438   Chem. Phys., 18, 11663-11682, https://doi.org/10.5194/acp-18-11663-2018, 2018.

439 Cerully, K. M., Bougiatioti, A., Hite, Jr., J. R., Guo, H., Xu, L., Ng, N. L., Weber, R., and Nenes, A.: On

440   the link between hygroscopicity, volatility, and oxidation state of ambient and water-soluble aerosols

441   in the southeastern United States, Atmos. Chem. Phys., 15, 8679–8694, 2015,

442   https://doi.org/10.5194/acp-15-8679-2015.

443 IPCC (Intergovernmental Panel on Climate Change): Climate Change 2013: The Physical Science Basis,

444   Summary for Policymakers, Cambridge University Press, Cambridge, UK and New York, 2013.

445 Kacarab, M., Thornhill, K. L., Dobracki, A., Howell, S. G., O'Brien, J. R., Freitag, S., Poellot, M. R., Wood,

446   R., Zuidema, P., Redemann, J., and Nenes, A.: Biomass burning aerosol as a modulator of the droplet

447   number in the southeast Atlantic region, Atmos. Chem. Phys., 20, 3029–3040,

448   https://doi.org/10.5194/acp-20-3029-2020, 2020.

449 Kalkavouras, P., Bossioli, E., Bezantakos, S., Bougiatioti, A., Kalivitis, N., Stavroulas, I., Kouvarakis, G.,

450   Protonotariou, A. P., Dandou, A., Biskos, G., Mihalopoulos, N., Nenes, A., and Tombrou, M.: New

451   particle formation in the southern Aegean Sea during the Etesians: importance for CCN production

452   and cloud droplet number, Atmos. Chem. Phys., 17, 175-192, https://doi.org/10.5194/acp-17-175-

453   2017, 2017.

454 Kalkavouras, P., Bougiatioti, A., Kalivitis, N., Stavroulas, I., Tombrou, M., Nenes, A., and Mihalopoulos,

455   N.: Regional new particle formation as modulators of cloud condensation nuclei and cloud droplet

456   number in the eastern Mediterranean, Atmos. Chem. Phys., 19, 6185–6203,

457   https://doi.org/10.5194/acp-19-6185-2019, 2019.

458 Kupc, A., Williamson, C., Wagner, N. L., Richardson, M., and Brock, C. A.: Modification, calibration, and

459   performance of the Ultra-High Sensitivity Aerosol Spectrometer for particle size distribution and

460   volatility measurements during the Atmospheric Tomography Mission (ATom) airborne campaign,

461   Atmos. Meas. Tech., 11, 369–383, https://doi.org/10.5194/amt-11-369-2018, 2018.

Lance, S., Nenes, A., Mazzoleni, C., Dubey, M. K., Gates, H., Varutbangkul, V., Rissman, T. A., Murphy, S. M., Sorooshian, A., Flagan, T. A., Seinfeld, J. H., Feingold, G., and Jinsson, H.: Cloud condensation nuclei activity, closure, and droplet growth kinetics of Houston aerosol during the Gulf of Mexico Atmospheric Composition and Climate Study (GoMACCS), J. Geophys. Res., 114, D00F15, doi:10.1029/2008JD011699, 2009.

Lathem, T. L., Beyersdorf, A. J., Thornhill, K. L., Winstead, E. L., Cubison, M. J., Hecobian, A., Jimenez, J. L., Weber, R. J., Anderson, B. E., and Nenes, A.: Analysis of CCN activity of Arctic aerosol and Canadian biomass burning during summer 2008, Atmos. Chem. Phys., 13, 2735-2756, https://doi.org/10.5194/acp-13-2735-2013, 2013.

Leibensperger, E. M., Mickley, L. J., Jacob, D. J., Chen, W.-T., Seinfeld, J. H., Nenes, A., Adams, P. J., Streets, D. G., Kumar, N., and Rind, D.: Climatic effects of 1950–2050 changes in US anthropogenic aerosols – Part 1: Aerosol trends and radiative forcing, Atmos. Chem. Phys., 12, 3333-3348, https://doi.org/10.5194/acp-12-3333-2012, 2012a.

Leibensperger, E. M., Mickley, L. J., Jacob, D. J., Chen, W.-T., Seinfeld, J. H., Nenes, A., Adams, P. J., Streets, D. G., Kumar, N., and Rind, D.: Climatic effects of 1950–2050 changes in US anthropogenic aerosols – Part 2: Climate response, Atmos. Chem. Phys., 12, 3349-3362, https://doi.org/10.5194/acp-12-3349-2012, 2012b.

Middlebrook, A. M., Bahreini, R., Jimenez, J. L., and Canagaratna, M. R.: Evaluation of composition-dependent collection efficiencies for the Aerodyne aerosol mass spectrometer using field data, Aerosol Sci. Tech., 46, 258–271, doi.org/10.1080/02786826.2011.620041, 2012.

Moore, R. H., Bahreini, R., Brock, C. A., Froyd, K. D., Cozic, J., Holloway, J. S., Middlebrook, A. M., Murphy, D. M., and Nenes, A.: Hygroscopicity and composition of Alaskan Arctic CCN during April 2008, Atmos. Chem. Phys., 11, 11 807–11 825, https://doi.org/10.5194/acp-11-11807-2011, 2011.

Moore, R. H., Cerully, K., Bahreini, R., Brock, C. A., Middlebrook, A. M., and Nenes, A.: Hygroscopicity and composition of California CCN during summer 2010, J. Geophys. Res., 117, https://doi.org/10.1029/2011JD017352, 2012.

Morales, R. and Nenes, A.: Characteristic updrafts for computing distribution-averaged cloud droplet number, autoconversion rate effective radius, J. Geophys. Res., 115, D18220, doi:10.1029/2009JD013233, 2010.

Morales Betancourt, R. and Nenes, A.: Droplet activation parameterization: the population-splitting concept revisited, Geosci. Model Dev., 7, 2345–2357, https://doi.org/10.5194/gmd-7-2345-2014, 2014a.

Morales Betancourt, R. and Nenes, A.: Understanding the contributions of aerosol properties and parameterization discrepancies to droplet number variability in a global climate model, Atmos. Chem. Phys., 14, 4809-4826, https://doi.org/10.5194/acp-14-4809-2014, 2014b.

Nenes, A. and Seinfeld, J.H.: Parameterization of cloud droplet formation in global climate models, J. Geophys. Res, 108, 4415, doi:10.1029/2002JD002911, 2003.

Petters, M. D. and Kreidenweis, S. M.: A single parameter representation of hygroscopic growth and cloud condensation nucleus activity, Atmos. Chem. Phys., 7, 1961–1971, doi:10.5194/acp-7-1961-2007, 2007.

Pringle, K. J., Tost, H., Pozzer, A., Pöschl, U., and Lelieveld, J.: Global distribution of the effective aerosol hygroscopicity parameter for CCN activation, Atmos. Chem. Phys., 10, 5241–5255, https://doi.org/10.5194/acp-10-5241-2010, 2010.

Quinn, P. K., Bates, T. S., Coffman, D. J., and Covert, D. S.: Influence of particle size and chemistry on the cloud nucleating properties of aerosols, Atmos. Chem. Phys., 8, 1029-1042, https://doi.org/10.5194/acp-8-1029-2008, 2008.

Reutter, P., Su, H., Trentmann, J., Simmel, M., Rose, D., Gunthe, S. S., Wernli, H., Andreae, M. O., and Pöschl, U.: Aerosol- and updraft-limited regimes of cloud droplet formation: influence of particle number, size and hygroscopicity on the activation of cloud condensation nuclei (CCN), Atmos. Chem. Phys., 9, 7067-7080, https://doi.org/10.5194/acp-9-7067-2009, 2009.

Seidel, D. J., Zhang, Y., Beljaars, A., Golaz, J.-C., Jacobson, A. R., and Medeiros, B.: Climatology of the planetary boundary layer over the continental United States and Europe, J. Geophys. Res., 117, D17106, doi:10.1029/2012JD018143, 2012.

Seinfeld, J., and Pandis, S.: Atmospheric Chemistry and Physics: From Air Pollution to Climate Change, John Wiley, Hoboken, N. J., 1998.

Seinfeld, J. H., Bretherton, C. S., Carslaw, K. S., Coe, H., De- Mott, P. J., Dunlea, E. J., Feingold, G., Ghan, S. J., Guenther, A.B., Kahn, R. A., Kracunas, I. P., Kreidenweis, S. M., Molina, M. J., Nenes, A., Penner, J. E., Prather, K. A., Ramanathan, V., Ramaswamy, V., Rasch, P. J., Ravishankara, A. R., Rosenfeld, D., Stephens, G., and Wood R.: Improving our fundamental understanding of the role of aerosol-cloud interactions in the climate system, Proc. Nat. Acad. Sci. USA, 113, 5781–5790, https://doi.org/10.1073/pnas.1514043113, 2016.

Sullivan, S.C., Lee, D., Oreopoulos, L., and Nenes, A.: The role of updraft velocity in temporal variability of cloud hydrometeor number, Proc. Nat. Acad. Sci, 113, 21, https://doi.org/10.1073/pnas.1514039113, 2016.

Wagner, N. L., Brock, C. A., Angevine, W. M., Beyersdorf, A., Campuzano-Jost, P., Day, D., de Gouw, J. A., Diskin, G. S., Gordon, T. D., Graus, M. G., Holloway, J. S., Huey, G., Jimenez, J. L., Lack, D. A.,

Liao, J., Liu, X., Markovic, M. Z., Middlebrook, A. M., Mikoviny, T., Peischl, J., Perring, A. E., Richardson, M. S., Ryerson, T. B., Schwarz, J. P., Warneke, C., Welti, A., Wisthaler, A., Ziemba, L. D., and Murphy, D. M.: In situ vertical profiles of aerosol extinction, mass, and composition over the southeast United States during SENEX and SEAC4RS: observations of a modest aerosol enhancement aloft, Atmos. Chem. Phys., 15, 7085-7102, https://doi.org/10.5194/acp-15-7085-2015, 2015.

Wang, J., Cubison, M. J., Aiken, A. C., Jimenez, J. L., and Collins,D. R.: The importance of aerosol mixing state and size-resolvedcomposition on CCN concentration and the variation of the im-portance with atmospheric aging of aerosols, Atmos. Chem.Phys., 10, 7267–7283,doi:10.5194/acp-10-7267-2010, 2010.

Warneke, C., Trainer, M., de Gouw, J. A., Parrish, D. D., Fahey, D. W., Ravishankara, A. R., Middlebrook, A. M., Brock, C. A., Roberts, J. M., Brown, S. S., Neuman, J. A., Lerner, B. M., Lack, D., Law, D., Hübler, G., Pollack, I., Sjostedt, S., Ryerson, T. B., Gilman, J. B., Liao, J., Holloway, J., Peischl, J., Nowak, J. B., Aikin, K. C., Min, K.-E., Washenfelder, R. A., Graus, M. G., Richardson, M., Markovic, M. Z., Wagner, N. L., Welti, A., Veres, P. R., Edwards, P., Schwarz, J. P., Gordon, T., Dube, W. P., McKeen, S. A., Brioude, J., Ahmadov, R., Bougiatioti, A., Lin, J. J., Nenes, A., Wolfe, G. M., Hanisco, T. F., Lee, B. H., Lopez-Hilfiker, F. D., Thornton, J. A., Keutsch, F. N., Kaiser, J., Mao, J., and Hatch, C. D.: Instrumentation and measurement strategy for the NOAA SENEX aircraft campaign as part of the Southeast Atmosphere Study 2013, Atmos. Meas. Tech., 9, 3063-3093, https://doi.org/10.5194/amt-9-3063-2016, 2016.

Wilson, J. C., Lafleur, B. G., Hilbert, H., Seebaugh, W. R., Fox, J., Gesler, D. W., Brock, C. A., Huebert, B. J., and Mullen, J.: Function and performance of a low turbulence inlet for sampling supermicron particles from aircraft platforms, Aerosol Sci. Tech., 38, 790–802, , https://doi.org/10.1080/027868290500841, 2004.

Weber RJ, Guo H, Russell AG, Nenes A.: High aerosol acidity despite declining atmospheric sulfate concentrations over the past 15 years, Nat. Geosci., 9, 282-285, https://doi.org/10.1038/ngeo2665, 2016.

Yu, S., Alapaty, K., Mathur, R., Pleim, J., Zhang, Y., Nolte, C., Eder, B., Foley, K., and Nagashima, T.: Attribution of the United States "warming hole": Aerosol indirect effect and precipitable water vapor. Sci. Rep., 4, 6929, https:// doi.org/10.1038/srep06929, 2014.

557 **Table 1:** Research flights from the SENEX 2013 campaign used in this study. The symbol "☼" next to
558 each flight number refers to daytime flight, and "☾" refers to a nighttime flight.

Flight	Date	Local Time (UTC-5)	Hygroscopicity Parameter κ	Organic mass fraction
4☼	10/6	09:55-16:30	0.23±0.02	0.62±0.11
5☼	11/6	11:30-17:57	0.20±0.00	0.68±0.05
6☼	12/6	09:48-15:31	0.21±0.01	0.68±0.07
9☾	19/6	17:30-23:29	0.24±0.01	0.66±0.06
10☼	22/6	10:01-17:09	0.21±0.02	0.68±0.08
11☼	23/6	10:08-17:22	0.25±0.03	0.58±0.07
12☼	25/6	10:18-17:25	0.39±0.02	0.35±0.18
14☼	29/6	10:26-17:39	0.22±0.03	0.62±0.07
15☾	2/7	20:08-02:51	0.28±0.05	0.55±0.09
16☾	3/7	19:56-02:55	0.22±0.05	0.67±0.09
17☼	5/7	09:52-16:24	0.23±0.05	0.59±0.14
18☼	6/7	09:19-16:18	0.31±0.02	0.52±0.08
19☼	8/7	10:11-16:44	0.23±0.04	0.62±0.08
Average			0.25±0.05	0.60±0.09

559

560

561

Table 2: Flight number, time interval, standard deviation of vertical wind velocity (σ_w) and characteristic vertical velocity $w^*=0.79\sigma_w$ during flight segments where the aircraft flew at a constant altitude.

Flight (pass)	Time Interval (Local Time)	σ_w (m s^{-1})	w^* (m s^{-1})	Altitude a.s.l. (m)	Flight (pass)	Time Interval (Local Time)	σ_w (m s^{-1})	w^* (m s^{-1})	Altitude a.s.l. (m)
5 (1)	12:31-12:58	1.02	0.81	549± 58	9 (1)	18:44-18:58	0.25	0.20	797±2.01
5 (2)	13:16-13:29	0.82	0.65	982±11	9 (2)	19:20-19:29	0.25	0.2	740±1.23
5 (3)	13:34-13:50	1.01	0.80	502±13	9 (3)	19:33-19:48	0.22	0.17	740±1.23
5 (4)	13:53-14:08	1.03	0.81	614±27	9 (4)	19:51-20:25	0.22	0.17	776±1.22
5 (5)	14:20-15:00	0.91	0.72	603±40	9 (5)	20:34-20:39	0.23	0.18	597±1.19
5 (6)	15:35-15:41	0.87	0.69	533±18	9 (6)	20:44-20:52	0.16	0.12	484±1.14
5 (7)	16:17-16:30	0.77	0.61	638±23	9 (7)	20:56-21:10	0.20	0.16	773±1.11
5 (8)	16:31-16:39	0.55	0.44	559±18	9 (8)	21:31-21:45	0.19	0.15	725±1.18
5 (9)	17:10-17:22	0.53	0.42	686±40	9 (9)	22:24-22:31	0.26	0.20	745± 1.36
					9 (10)	22:48-22:54	0.22	0.17	804± 1.37
14 (1)	12:34-12:49	0.94	0.75	558±2	15 (1)	21:09-21:52	0.24	0.19	505±6.64
14 (2)	13:57-14:17	0.97	0.77	658±3	15 (2)	22:19-22:31	0.30	0.24	633±1.21
14 (3)	14:22-14:46	0.95	0.75	737±3	15 (3)	22:42-22:54	0.25	0.20	600±1.17
14 (4)	14:58-15:33	0.55	0.43	746±23	15 (4)	23:26-23:37	0.33	0.26	908±1.56
14 (5)	15:55-16:08	0.57	0.45	714±3	15 (5)	00:02-00:19	0.30	0.23	1208±1.23
14 (6)	16:11-16:21	0.77	0.61	801±3	15 (6)	00:43-1:08	0.25	0.20	592±1.37
14 (7)	16:33-16:41	0.45	0.35	793± 2	15 (7)	1:10-1:24	0.28	0.22	676±1.02
					15 (8)	1:37-2:02	0.21	0.16	713±19.5
12 (1)	11:50-12:34	0.96	0.75	484±3	19 (1)	11:20-11:41	0.62	0.49	1014±2.27
12 (2)	12:48-13:18	1.09	0.86	503±3	19 (2)	12:09-12:23	1.20	0.95	652±3.34
12 (3)	13:34-13:50	1.12	0.88	894±3	19 (3)	12:51-13:10	0.87	0.69	537±2.51
12 (4)	14:06-14:40	1.04	0.82	479±4	19 (4)	13:22-13:49	1.29	1.02	518±22.6
12 (5)	15:21-15:32	1.10	0.87	521±3	19 (5)	14:44-14:57	1.36	1.07	528±3.26
12 (6)	15:43-16:02	0.99	0.78	475±3	19 (6)	15:04-16:06	0.90	0.71	524±2.8

Table 3: Derived cloud parameters (maximum supersaturation, droplet number) and relative contribution (Equation 2) of chemical composition
and total aerosol number for different vertical velocities. Numbers in parentheses indicate standard deviation values. The symbol "☼" next to each
flight number refers to daytime flight, and "☾" refers to a nighttime flight.

569

Flight	N_a	Std Dev N_a	σ_w=0.1 m s^{-1}				σ_w=0.3 m s^{-1}				σ_w=0.6 m s^{-1}				σ_w=1.0 m s^{-1}			
			S_{max}	N_d	Contrib κ	Contrib N_a	S_{max}	N_d	Contrib κ	Contrib N_a	S_{max}	N_d	Contrib κ	Contrib N_a	S_{max}	N_d	Contrib κ	Contrib N_a
4☼	6118	4520	0.11 (0.06)	122 (41)	0.08	0.92	0.16 (0.09)	315 (114)	0.20	0.80	0.21 (0.12)	520 (212)	0.23	0.77	0.26 (0.17)	737 (321)	0.2	0.8
5☼	4324	2598	0.08 (0.04)	139 (31)	0.09	0.91	0.1 (0.06)	388 (104)	0.15	0.85	0.14 (0.08)	712 (216)	0.17	083	0.17 (0.1)	1063 (360)	0.21	0.79
6☼	4958	3054	0.07 (0.07)	151 (24)	0.03	0.97	0.08 (0.04)	422 (70)	0.11	0.89	0.1 (0.06)	773 (171)	0.08	0.92	0.13 (0.07)	1162 (302)	0.07	0.93
9☾	4271	3095	0.07 (0.02)	152 (18)	0.05	0.95	0.12 (0.04)	367 (68)	0.17	0.83	0.16 (0.05)	533 (115)	0.17	0.83	0.19 (0.06)	680 (126)	0.12	0.88
10☼	6286	7201	0.07 (0.03)	158 (24)	0.02	0.98	0.1 (0.05)	422 (86)	0.02	0.98	0.14 (0.07)	748 (180)	0.04	0.96	0.18 (0.08)	1063 (295)	0.09	0.91
11☼	5969	7271	0.04 (0.01)	137 (19)	0.01	0.99	0.06 (0.01)	381 (61)	0.04	0.96	0.08 (0.02)	695 (134)	0.03	0.97	0.10 (0.02)	1025 (226)	0.03	0.97
12☼	3154	5150	0.06 (0.03)	110 (45)	0.03	0.97	0.1 (0.04)	274 (117)	0.05	0.95	0.14 (0.04)	404 (179)	0.08	0.92	0.17 (0.05)	486 (207)	0.07	0.93
14☼	5564	5891	0.07 (0.02)	118 (41)	0.05	0.95	0.10 (0.03)	328 (125)	0.17	0.83	0.13 (0.04)	590 (240)	0.25	0.75	0.16 (0.05)	842 (361)	0.27	0.73
15☾	2328	1428	0.05 (0.01)	135 (22)	0.03	0.97	0.09 (0.02)	339 (67)	0.12	0.88	0.12 (0.02)	557 (137)	0.21	0.79	0.16 (0.03)	717 (203)	0.3	0.7
16☾	3440	4507	0.08 (0.06)	158 (37)	0.03	0.97	0.12 (0.1)	403 (120)	0.06	0.94	0.17 (0.13)	670 (235)	0.07	0.93	0.23 (0.16)	917 (374)	0.1	0.9
17☼	3813	4645	0.05 (0.02)	129 (41)	0.06	0.94	0.07 (0.03)	342 (130)	0.1	0.9	0.1 (0.04)	593 (248)	0.06	0.94	0.13 (0.05)	841 (371)	0.06	0.94
18☼	1925	983	0.08 (0.04)	90 (58)	0.12	0.88	0.12 (0.05)	233 (157)	0.35	0.65	0.15 (0.06)	379 (262)	0.37	0.63	0.19 (0.07)	499 (346)	0.27	0.73
19☼	4323	7261	0.06 (0.02)	121 (33)	0.02	0.98	0.08 (0.02)	314 (96)	0.06	0.94	0.12 (0.03)	526 (177)	0.11	0.89	0.15 (0.03)	670 (249)	0.13	0.87

570

571

Table 4: Derived S_{max}, N_d, σ_w for all research flights along with the estimated contribution of each parameter to the variability of the droplet number. The symbol "☼" next to each flight number refers to daytime flight, and "☾" refers to a nighttime flight.

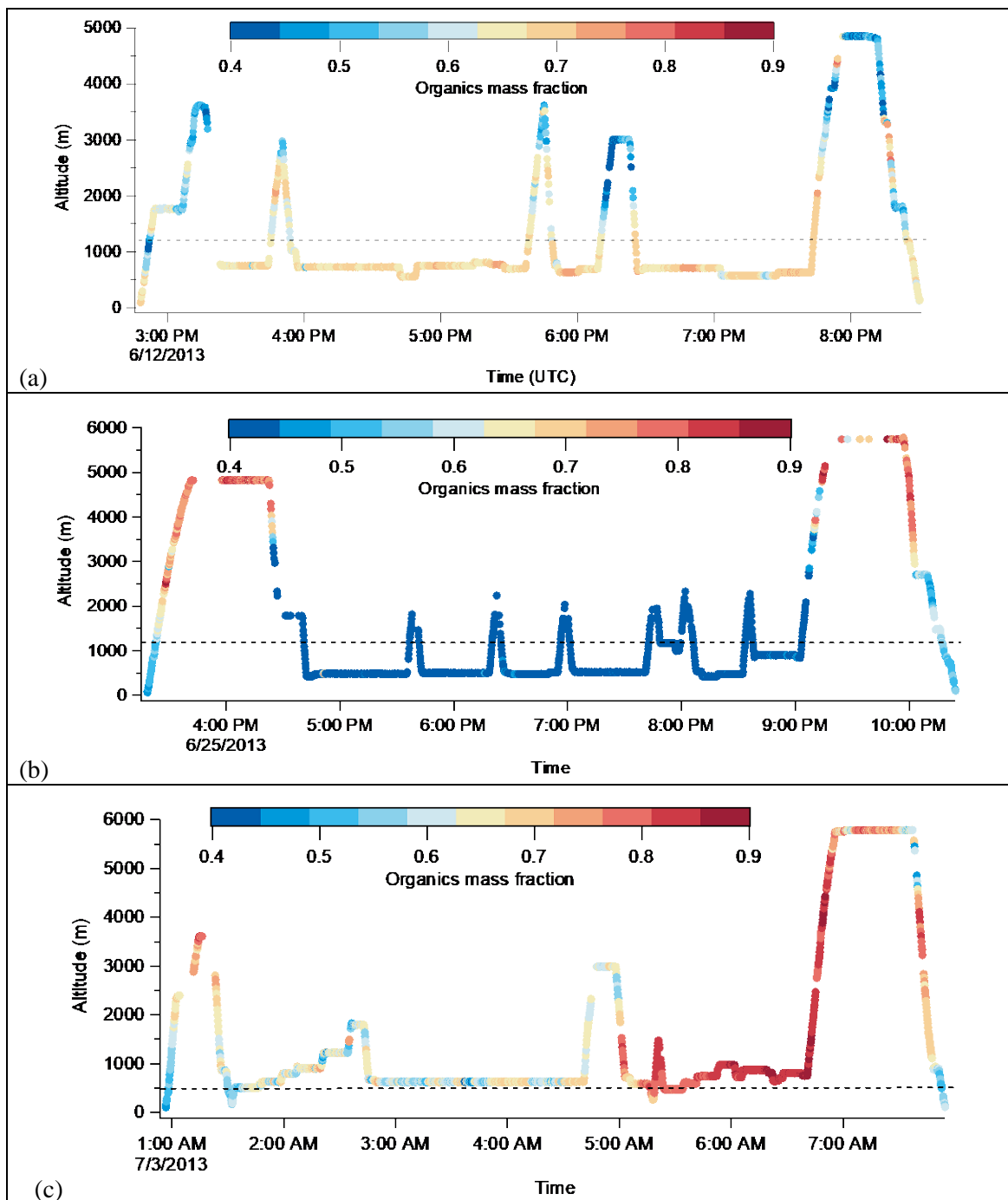| Flight	σ_w (m s⁻¹)	$\dfrac{\Delta\sigma_w}{\sigma_w}$	S_{max} (%)	N_d (cm⁻³)	$\dfrac{\Delta N_d}{N_d}$	Contrib. κ	Contrib. N_a	Contrib. σ_w
4☼	1.03±0.25	0.243	0.29±0.19	707±343	0.485	4%	79%	17%
5☼	0.97±0.1	0.103	0.17±0.10	1040±350	0.337	7%	69%	24%
6☼	0.94±0.18	0.191	0.13±0.07	1108±283	0.255	3%	54%	43%
9☾	0.23±0.02	0.043	0.10±0.03	309±51	0.165	7%	76%	17%
10☼	1.22±0.11	0.090	0.12±0.03	1177±271	0.230	1%	90%	9%
11☼	1.08±0.04	0.037	0.11±0.03	1082±242	0.224	1%	83%	16%
12☼	1.05±0.07	0.067	0.18±0.05	495±210	0.424	2%	96%	2%
14☼	0.85±0.2	0.024	0.15±0.04	761±321	0.422	9%	72%	19%
15☾	0.28±0.04	0.143	0.08±0.02	321±63	0.196	7%	51%	42%
16☾	0.20±0.04	0.200	0.10±0.08	289±79	0.273	2%	65%	33%
17☼	0.71±0.26	0.366	0.15±0.11	742±280	0.377	1%	71%	28%
18☼	0.90±0.06	0.067	0.31±0.18	538±325	0.604	7%	83%	10%
19☼	0.99±0.31	0.313	0.15±0.03	699±248	0.355	4%	88%	8%
Average					0.334	4%	75.2%	20.6%

Figure 1: Altitude as a function of time (UTC) colored by organic mass fraction. Spatial and vertical distribution of the organics mass fraction (a) for Flight 6, (b) for Flight 12 and (c) for Flight 16, denoting the difference in chemical composition, which in turn, may influence cloud droplet number concentration. The dashed line represents the boundary layer height, derived from Wagner et al., (2015) for daytime (1200 m) and from Seidel et al., (2012) for nighttime (500 m).
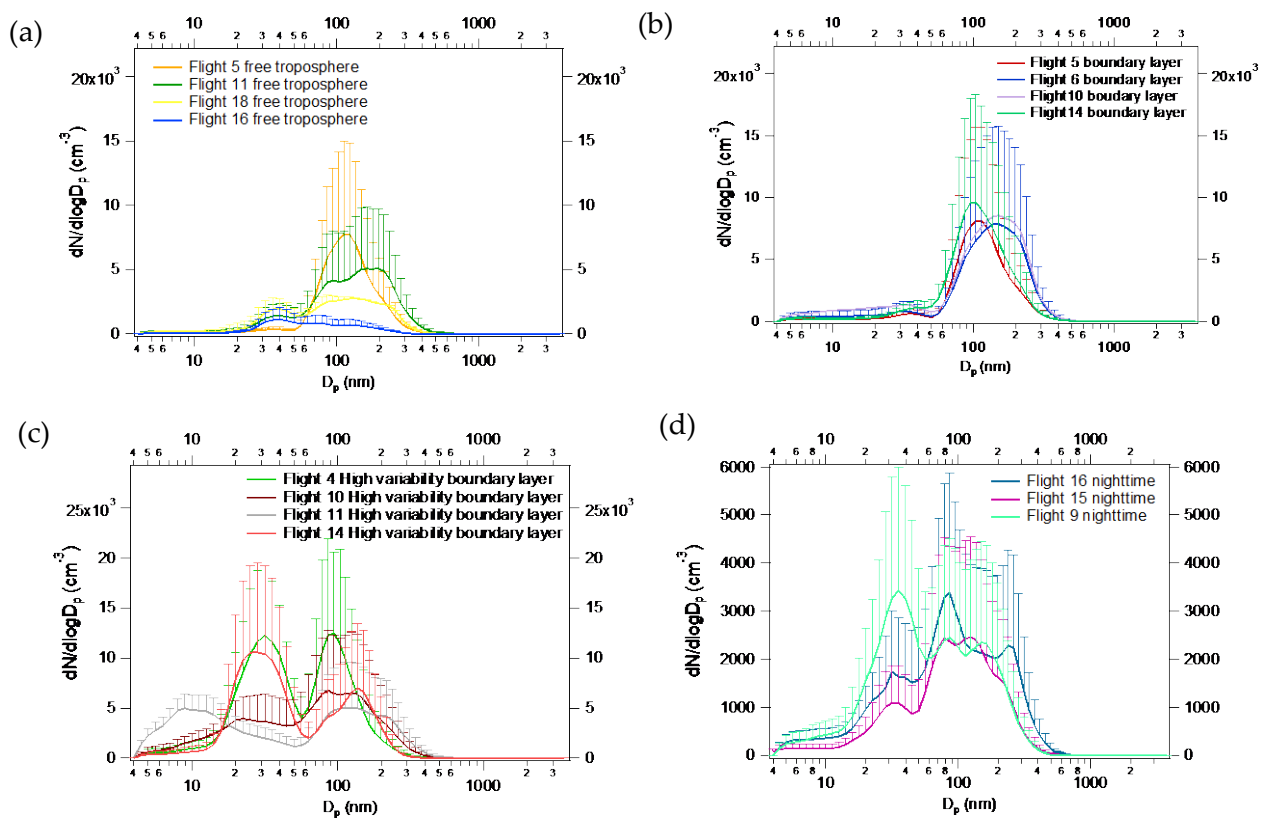
Figure 2: Average particle number size distributions for: (a) free tropospheric conditions, (b) within the boundary layer, (c) during segments with high variability in total aerosol number, and (d) during nighttime passes. Error bars represent the 75th percentile of the distributions within each segment.
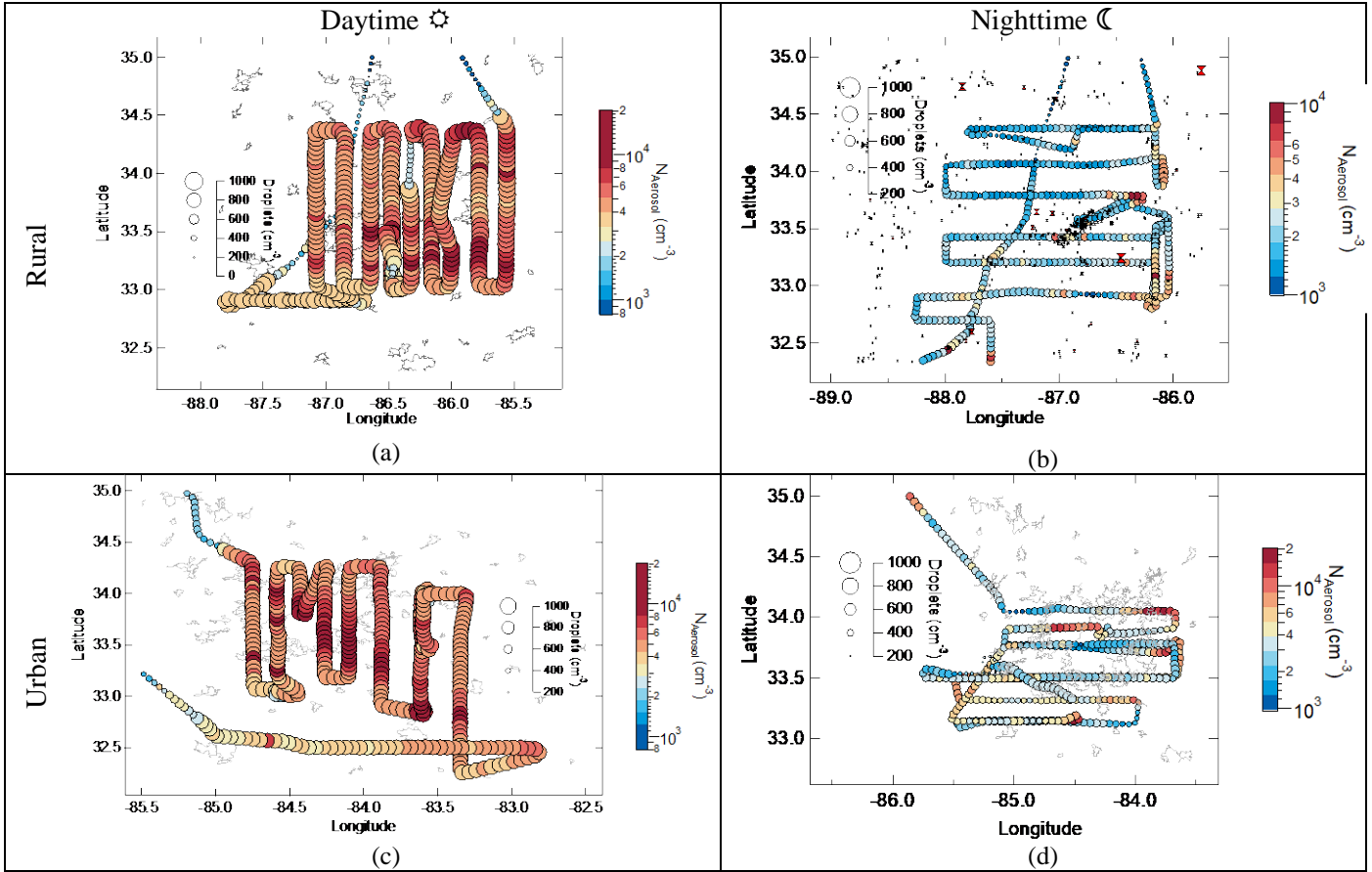
Figure 3: Map of aircraft flight track showing calculated cloud droplet number (indicated by marker size (cm^{-3})) and total aerosol number (indicated by marker color) for the observed characteristic vertical velocity ($w*$). (a) for the rural sector during daytime (Flight 5) and (b) nighttime (Flight 15). (c) for urban Atlanta during daytime (Flight 6) and (d) nighttime (Flight 9). Note that the data are plotted at less than 1 Hz in order to better show the size and color of the markers.
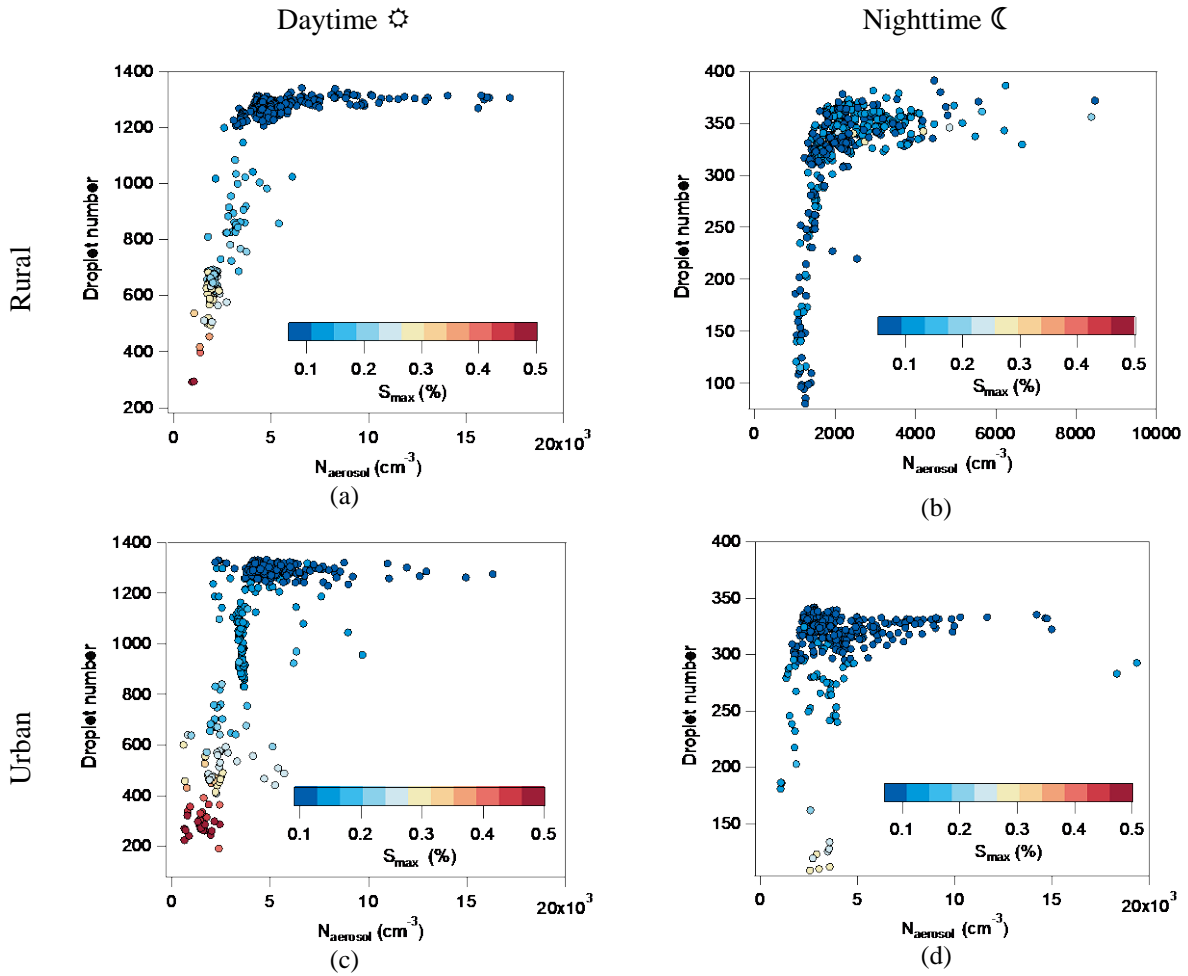
Figure 4: Cloud droplet number vs. total aerosol number for the derived characteristic vertical velocity (*w**) of each flight (Table 4). (a) for the rural sector during daytime (Flight 5) and (b) nighttime (Flight 15). (c) for urban Altanta during daytime (Flight 6) and (d) nighttime (Flight 9). Data are colored by maximum supersaturation.
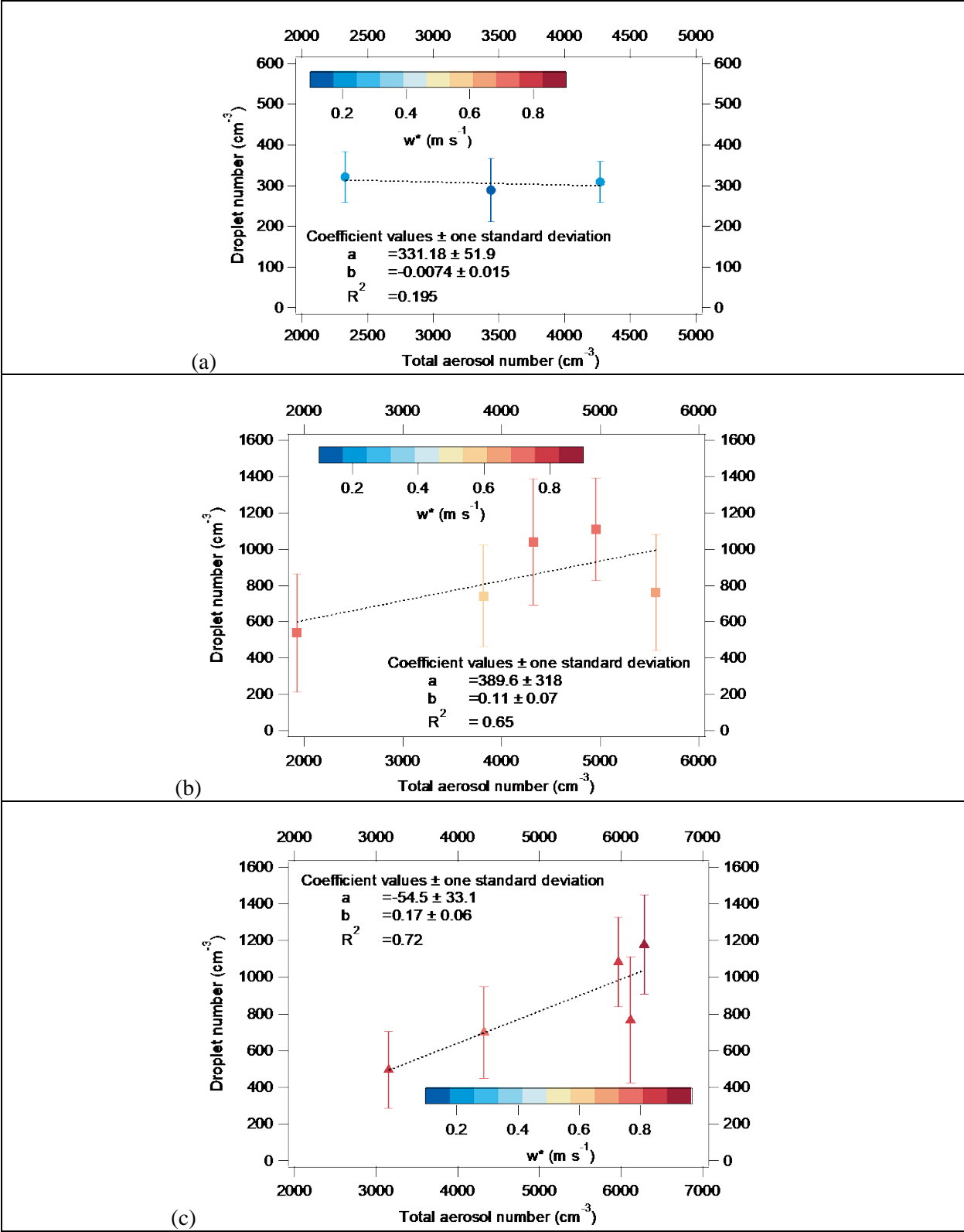
Figure 5: Average cloud droplet number vs. total aerosol number, colored by characteristic velocity w* for each flight. Error bars represent the standard deviation of cloud droplet number during each flight.
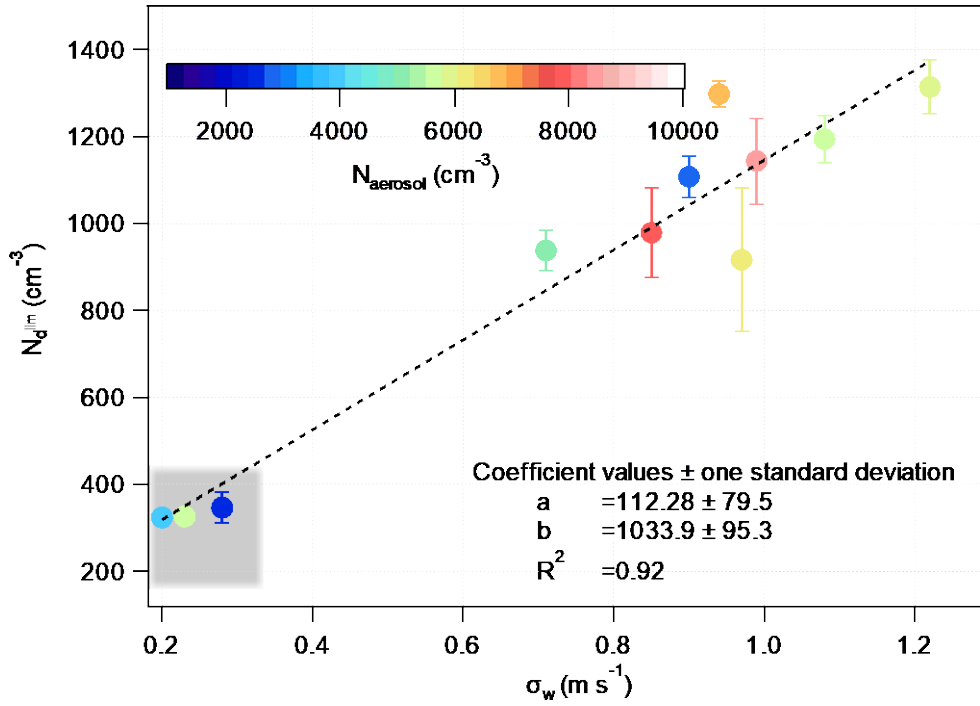
Figure 6: Limiting droplet number vs. standard deviation of vertical velocity during flights where a velocity-limited regime is reached (all except Flights 4, 12). The shaded area represents the segments of the flights conducted during nighttime while color scale denotes total aerosol number levels.